Computers and Fluids 173 (2018) 140–146

Contents lists available at ScienceDirect

Computers and Fluids

journal homepage: www.elsevier.com/locate/compfluid

Large-scale molecular dynamics simulation of flow under complex structure of endothelial glycocalyx

Xi Zhuo Jiang*, Muye Feng, Kai H. Luo*, Yiannis Ventikos*

Department of Mechanical Engineering, University College London, Torrington Place, London WC1E 7JE, UK

ARTICLE INFO

Article history:
Received 30 July 2017
Revised 7 February 2018
Accepted 1 March 2018
Available online 5 March 2018

Keywords:
Large-scale
Molecular dynamics
Flow
Endothelial glycocalyx
Complex structure

ABSTRACT

In this research, large-scale molecular dynamics (MD) simulations were conducted to study the fluid dynamics inside the endothelial glycocalyx layer. A work flowchart regarding constructing the flow/glycocalyx system, undertaking production simulation using the MD method and post-processing was proposed. Following the flowchart, physiological and accelerating flow cases were simulated to reveal velocity and shear stress distributions over the dendritic (tree-like) structure of the glycocalyx, thereby contributing to understanding of the influence of biomolecular complex structures on flow profiles. Besides, the selection of thermostat algorithm was discussed. Results have shown that when the forcing is below a critical value, the velocity fluctuates around a zero mean along the height in the presence of the dendritic glycocalyx. When the forcing is larger than a critical value, the bulk flow was accelerated excessively, departing from the typical physiological flow. Furthermore, distributions of shear stress magnitude among three sub-regions in the ectodomain indicate that shear stress is enhanced near the membrane surface but is impaired in the sugar-chain-rich region due to the flow regulation by sugar chains. Finally, comparisons of velocity evolutions under two widely used thermostats (Lowe-Andersen and Berendsen thermostats) imply that the Lowe-Andersen algorithm is a suitable thermostat for flow problems.

1. Introduction

Human metabolism requires exchange of materials between circulating blood and tissues. The material exchange occurs across a thin layer of endothelial cells located in the luminal surface of the blood vessels, known as the endothelium. The endothelium cells line the entire vascular network, from the wide heart arteries to the smallest capillaries [1]. The glycocalyx, a network of membrane-bound proteoglycans and glycoproteins, is located on the apical surface of vascular endothelial cells and is the first barrier in direct contact with blood [2]. The endothelial glycocalyx layer is related to many cardiovascular and renal diseases or illness, such as diabetes [3], ischemia/reperfusion [4], and atherosclerosis [5].

Electron micrograph of endothelium shows that the endothelial glycocalyx features its dendritic (tree-like) structure [6,7] and is exposed to the blood flow. To better understand the pathologies of glycocalyx-related cardiovascular diseases, the flow profile under the dendritic structure of the glycocalyx should be resolved. However, few firm conclusions about flow profiles in the presence of complex structures can be obtained from classic fluid mechanics and experiments. Therefore, researchers turn to computational methods for new insights.

One of the most powerful computational *in silico* techniques is molecular dynamics (MD) simulation, which can provide the trajectories of all atoms by solving Newton's Second Law of Motion. Although MD simulations have contributed to contemporary understanding of the glycocalyx, the lack of structural information of the glycocalyx has impeded the field for a long period. Not until recently was the most detailed structural information of the glycocalyx [8] published, which provides the feasibility to thoroughly study the flow structures in the presence of the complex configurations of the glycocalyx.

In this research, large-scale molecular dynamics simulations will be conducted to study the flow profile under the dendritic structure of the endothelial glycocalyx. Work flowchart regarding procedure of establishing flow/glycocalyx system, conducting simulations using the MD method and post-processing will be first proposed. Following the flowchart, physiological and accelerating flow cases will be undertaken to provide new insights into the influence of biomolecular structural configurations on flow profiles. Finally, selection of thermostat algorithm will be discussed.

* Corresponding authors.
E-mail addresses: xizhuo.jiang.14@ucl.ac.uk (X.Z. Jiang), k.luo@ucl.ac.uk (K.H. Luo), y.ventikos@ucl.ac.uk (Y. Ventikos).

https://doi.org/10.1016/j.compfluid.2018.03.014

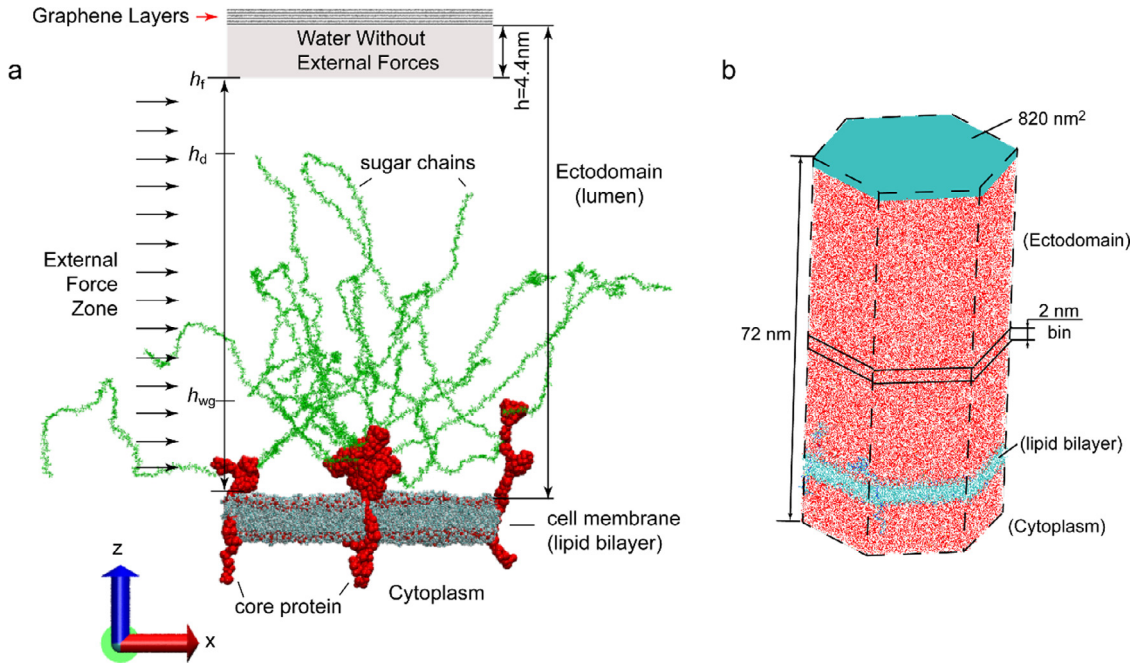

Fig. 1. Initial configuration of the all-atom glycocalyx-flow system and perspective view of the simulation box. (a) Initial configuration. The system includes 3 Syn-4 dimers as proteoglycan, 18 sugar chains attached on the apexes of Syn-4 dimers and a lipid bilayer. External forces are imposed in the x direction on the water molecules in the ectodomain. Water molecules and ions are not shown. Graphene layers are added at the top to prevent the water molecules propagating from ectodomain to the cytoplasm due to the periodic boundary conditions. In Panel a, h_{wg}, h_d and h_f represent the heights of near wall region, dendritic region and flow region, respectively. (b) Perspective view of the simulation box. An illustration of a bin used for post-processing is also provided.

For the first time, the flow and glycocalyx interactions are studied under both typical physiological and accelerating (like in a disease situation) flow situations. This research will contribute to the study of fluid mechanics by unveiling the flow behaviour in the presence of complex boundaries with moving soft structures. It also contributes to biomedical research through a better understanding of flow under normal and diseased situations that would affect the function of glycocalyx, potentially leading to therapeutic strategies for glycocalyx-related cardiovascular diseases.

2. Methods

2.1. System construction

The current most detailed structure of glycocalyx [8] has been adopted to build the flow/glycocalyx system [9]. In the system, Syndecan-4 (Syn-4) proteoglycan and heparin sulfate (HS) sugar chains are selected to model the glycocalyx. The glycocalyx structure can be divided into three parts: Syn-4 ectodomain linked with sugar chains; Syn-4 transmembrane dimer embedded into a lipid bilayer; and Syn-4 cytoplasmic dimer.

The initial configuration of the glycocalyx-flow system is illustrated in Fig. 1a. The whole space is divided into two compartments by the lipid bilayer. Above the lipid bilayer is the ectodomain, representing the lumen where flow passes by. This region contains HS sugar chains, Syn-4 ectodomain in connection with HS sugar chains, water molecules and ions. Below the lipid bilayer is the cytoplasm, representing the inner space of the cell, which is filled with Syn-4 cytoplasmic protein, water molecules and ions. All the biomolecules are solvated and ionized to 0.1 M NaCl aqueous solution. In the follow-on simulations, the periodic boundary conditions are applied to all the three directions. The application of the boundary conditions would cause water molecules to propagate from the upper boundary of the ectodomain to the lower boundary of the cytoplasm, and vice versa. This propagation would disturb the micro environment of the ectodomain and the cytoplasm. Thus, to prevent the disturbance, fixed graphene layers are added on the top of ectodomain. This practice has also been adopted in Cruz-Chu's study [8].

In the system, three proteoglycans which individually consist of one Syn-4 dimer are embedded in the lipid bilayer. Each proteoglycan has six sugar chains attached on the dimer apexes. To mimic flow, external forces are imposed on the water molecules in the ectodomain. The simulation box is a hexagonal prism with an area of 820 nm^2 and height of 72 nm (Fig. 1b). The glycocalyx-flow system comprises 5,800,000 atoms in total.

2.2. Work flow

A typical work flow to study flow problems using MD simulations can be divided into three procedures, as illustrated in Fig. 2. Equilibrium should be first reached to ensure structural stability of the biomolecules, before flow simulations are conducted. External forces are then imposed to water oxygens in the ectodomain to mimic the blood flow in the lumen. The order of physiological values of velocities for endothelial glycocalyx layers is expected to be mm/s to cm/s [10]. Thus, to generate physiological velocity, iterations of forces are required. When the time-evolution of the resulting bulk flow velocities is in physiological ranges, post-processing including the distributions of velocities and shear stresses is conducted for further data analysis. The packages or platforms involved in the flowchart for this research are also listed in Fig. 2.

2.3. Protocol details

The TIP3P water model [11] was adopted to simulate water molecules. A CHARMM biomolecular force field [12] was applied on the proteins and the lipid bilayer. Force field parameters for sugar chains and graphene layers were adopted from a previous study [8].

In accordance with the work flow in Fig. 2, an equilibrium simulation with graphene layers being fixed was conducted at con-

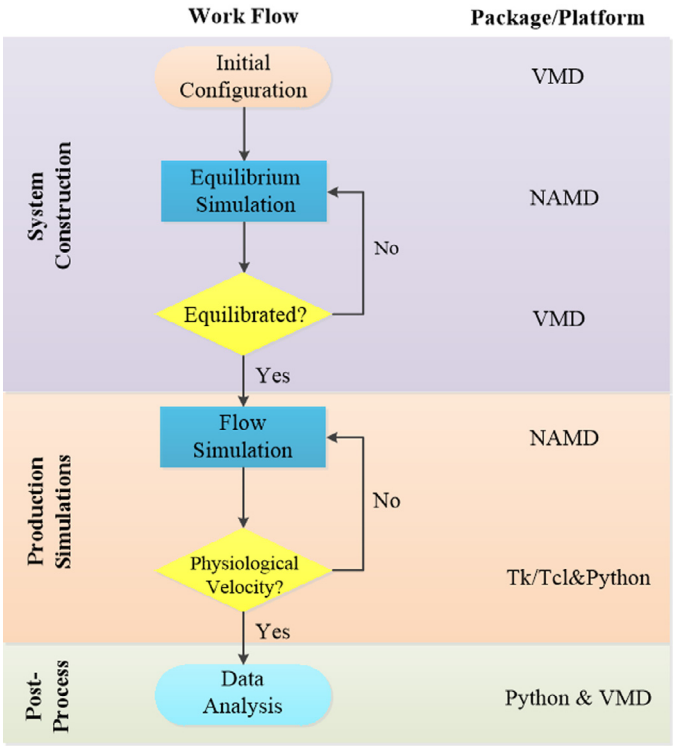

Fig. 2. Work flow and package/platform involved in large-scale molecular dynamics simulations to study flow profiles under the dendritic structure of the glycocalyx. NAMD 2.9 [16] and VMD [17] are adopted.

stant 1 atm and 310 K (NPT ensemble), using a Langevin thermostat and a Nosé-Hoover Langevin piston for 2 ns, followed by another simulation using a Langevin thermostat to maintain temperature at 310 K for 0.5 ns (NVT ensemble). The last frame of the NVT simulation was then used as the initial configuration (as shown in Fig. 1a) of the follow-up "production" flow simulations. In the flow simulations, the Lowe-Andersen thermostat was selected to maintain the temperature at 310 K.

In the flow simulations, the velocity Verlet integration method [13] was used to advance the positions and velocities of the atoms in time. A 2-fs timestep, and particle mesh Ewald [14] electrostatics with a grid density of $1/Å^3$ are used. The SETTLE algorithm [15] was used to enable the rigid bonds connected to all hydrogen atoms. The van der Waals interactions were calculated using a cutoff of 12 Å with a switching function starting at 10 Å.

All MD simulations were performed using the software NAMD 2.9 [16]. The visualisation of the molecular structures was performed by the VMD [17] package. Post-processing of the MD results was accomplished using PYTHON (Python Software Foundation, Wilmington, De) scripts. All parallel simulations and non-visualised post-processing were conducted on ARCHER, UK's national supercomputing service. To obtain a simulation result with physical time of 1 ns, 9,000 compute cores have been simultaneously employed for about 2 hours.

2.4. Binning and geometric division

To investigate the spatial distributions of flow velocity and shear stresses, a space with 50 nm height in the ectodomain is sliced into 25 equal bins (Fig. 1b). The height origin of the ectodomain space is determined by the average positions of heavy atoms (nitrogen and phosphor atoms) of the upper lipid heads, which has been reported in Ref. [9]. Within each bin, the flow velocity and shear stresses are to be calculated.

To include the effects of biomolecules on flow, the ectodomain of the system is divided into three sub-regions along the z direction in terms of molecule varieties therein: near wall region (wg), dendritic region (d) and flow region (f). The near wall region, starting from the upper surface of the lipid bilayer and ending at the apex of Syn-4, contains Syn-4 ectodomain, a few sugar chains, water molecules and ions. The dendritic region, from the apex of Syn-4 to the furthest end of the sugar chains and containing sugar chains, water molecules and ions, features its tree-like structure. The flow region, above the dendritic region, only includes water molecules and ions. The dimension of each sub-region is determined by the steric information of hallmark biomolecules during the 30-ns physiological simulation. The heights of the near wall sub-region and the dendritic sub-region are 12 (h_{wg} in Fig. 1a) and 36 nm (h_d in Fig. 1a), together with h_f equalling 50 nm as designated.

2.5. Calculations of shear stress component and magnitude

The focus of our attention in this research is one component of the stress tensor- the shear stress on the plane normal to x-axis in the z direction- τ, which is calculated by Eq. (1)

$$\tau = \mu \frac{\partial v_x}{\partial z} \tag{1}$$

where μ is the viscosity of the TIP3P water model (0.321 mPa s) [18]; and $\partial v_x/\partial z$ is the gradient of the x velocity along the z axis.

Discrete form by the forward difference method is used to calculate the shear stress in Eq. (1), as shown in Eq. (2).

$$\tau_i = \mu \frac{v_{x,i+1} - v_{x,i}}{z_{i+1} - z_i} \tag{2}$$

where index i $(0 < i < 25)$ represents the ith bin defined in Section 2.4, and the denominator, indeed, is the height of each bin (2 nm).

The shear stress in each sub-region (τ_{wg}, τ_d, and τ_f) is then calculated by averaging bin shear stresses therein. For example, the near-wall region is 12 nm in height and contains 6 bins. For a certain instant, the average shear stress in the near-wall region, τ_{wg}, is calculated as

$$\tau_{wg} = \frac{1}{5}\sum_{i=1}^{5} \tau_i \tag{3a}$$

Analogously, average shear stresses in the dendritic and flow sub-regions are calculated by Eqs. (3b) and (3c), respectively.

$$\tau_d = \frac{1}{11}\sum_{i=7}^{17} \tau_i \tag{3b}$$

$$\tau_f = \frac{1}{6}\sum_{i=19}^{24} \tau_i \tag{3c}$$

Correspondingly, the magnitudes of the three sub-regional shear stresses are obtained by Eqs. (4a)–(4c).

$$|\tau_{wg}| = \left|\frac{1}{5}\sum_{i=1}^{5} \tau_i\right| \tag{4a}$$

$$|\tau_d| = \left|\frac{1}{11}\sum_{i=7}^{17} \tau_i\right| \tag{4b}$$

$$|\tau_f| = \left|\frac{1}{6}\sum_{i=19}^{24} \tau_i\right| \tag{4c}$$

For both physiological and accelerating flow cases, the sub-regional shear stresses are recorded every 0.1 ns, thus shear stresses at every instant in each sub-region constitute an array.

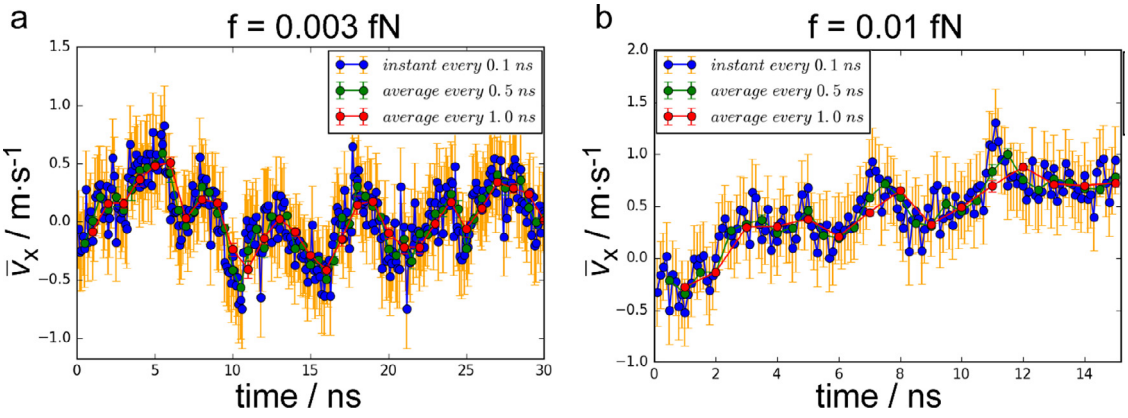

Fig. 3. Velocity evolutions under varying external forces. (a) Velocity evolution for a steady flow with physiological velocity values and the external force on each water oxygen atom being 0.003 fN. (b) Velocity evolution for accelerating flow with the external force on each water oxygen atom being 0.01 fN.

3. Results

3.1. Velocity evolutions

To generate a physiological flow, we first hierarchically decreased the external force on every oxygen atom of water molecules in the ectodomain. Results showed that, with external forces of 0.002 fN–0.0035 fN, the average bulk flow velocity in the x direction, $\bar{v}_x$, assumes values of a few cm/s, as expected. Thereafter, we selected 0.003 fN as the external force, and prolonged the flow simulation time to 30 ns for further extensive data exploration. An accelerating flow case with external force of 0.01 fN, aiming to explore abnormal scenarios in human bodies, was also included in this research. The accelerating case was conducted for a physical time of 15 ns, for $\bar{v}_x$ in the last 5 ns is approaching 1 m/s (as shown in Fig. 3b) which is typical for most abnormal situations [19]. Both flow cases share a common initial configuration. As shown in Fig. 3a, the bulk flow velocity of the physiological flow case (f = 0.003 fN) fluctuates around 0, which implies that the external force just counteracts the internal force originating from the interactions between water and surrounding molecules. When external force increases to 0.01 fN (Fig. 3b), the external force overwhelms the internal force, resulting in an increasing velocity trend with time.

3.2. Velocity distribution

The spatial velocity distributions in the ectodomain are then investigated. By averaging the x-direction velocities of water molecules in each layer every 5 ns, spatial velocity distributions along the height can be obtained. To facilitate comparisons, only the first 15-ns results of the physiological case (f = 0.003 fN) are adopted in this section. As shown in Fig. 4, velocities exhibit fluctuating distributions in the presence of glycocalyx for both physiological and accelerating flow cases, which can be attributed to continuous disturbance and steric obstacle from the glycocalyx atoms to water flow. In the accelerating flow case, the acceleration of the flow with time can also be observed as bulk velocity increases.

3.3. Shear stress distribution

Cumulative density functions (CDFs) of the sub-regional shear stress magnitudes for both cases are calculated in Fig. 5a and b, respectively. Results indicate that shear stress is enhanced in the near-wall region with lowest cumulative density for weak shear stress, which is consistent with previous theoretical prediction [20]. By contrast, shear stress in the dendritic region where sugar chains dominate is impaired with highest cumulative density for weak shear stress. The shear stress distributions can be explained by the complex configuration of glycocalyx. In the near-wall region, extensive interactions between the lipid bilayer and the adjacent water molecules as well as the disturbance from the ectodomain protein will act through friction-like effect to the flow and result in an obvious gradient of the x velocity along the z axis within the layer. Further dissection of the enhanced shear stresses (Fig. 5c) implies that the friction-like effect is especially significant for the physiological flow case where the external and internal forces are well-matched. While, in the dendritic region, the flexible sugar chains dissipate the kinetic energy of the fluid via frequent interactions with the water molecules, thereby disturbing the motions of water molecules and reducing the gradient of the x velocity along the z axis. As shown in Fig. 5d, the energy dissipation is particularly remarkable for the accelerating flow case, since the probability difference aggravates as the magnitude of weak shear stress decreases from 0.75 to 0.1.

4. Discussion

4.1. Selection of thermostat

Specifying the temperature in MD simulations involves using a "thermostat" that couples the system to an external heat bath. In this research, we use the Lowe-Andersen thermostat [21], a momentum conserving and Galilean invariant thermostat, which is advantageous in nonequilibrium simulations [22], like flow simulations. Meanwhile, the Berendsen thermostat [23], as often used in previous non-equilibrium MD studies [24–26], is an algorithm to re-scale the velocities of particles in the simulation system to control the temperature. The precise influence of thermostat methods on the MD results is still not fully understood, but previous studies have shown that the algorithms of thermostat can alter the dynamics of the system with the microcanonical ensemble by damping the diffusion and rotational motion of molecules in the simulation [27,28]. Furthermore, different algorithms adjust particle velocities in various ways, resulting in significant discrepancies in dynamic properties [28,29].

In this section, we compare average bulk flow velocities from the Lowe-Andersen and Berendsen thermostats. Six-nanosecond results are extracted with the external force on each water oxygen atom being 0.003 fN (Fig. 6). As shown in Fig. 6, average bulk flow velocity from the Lowe-Andersen has a larger mean than its Berendsen counterpart (p-value = 2.0×10^{-5} by T-test).

In the algorithm of the Berendsen thermostat [23], particle velocities are scaled at each step so that the entire system is set to

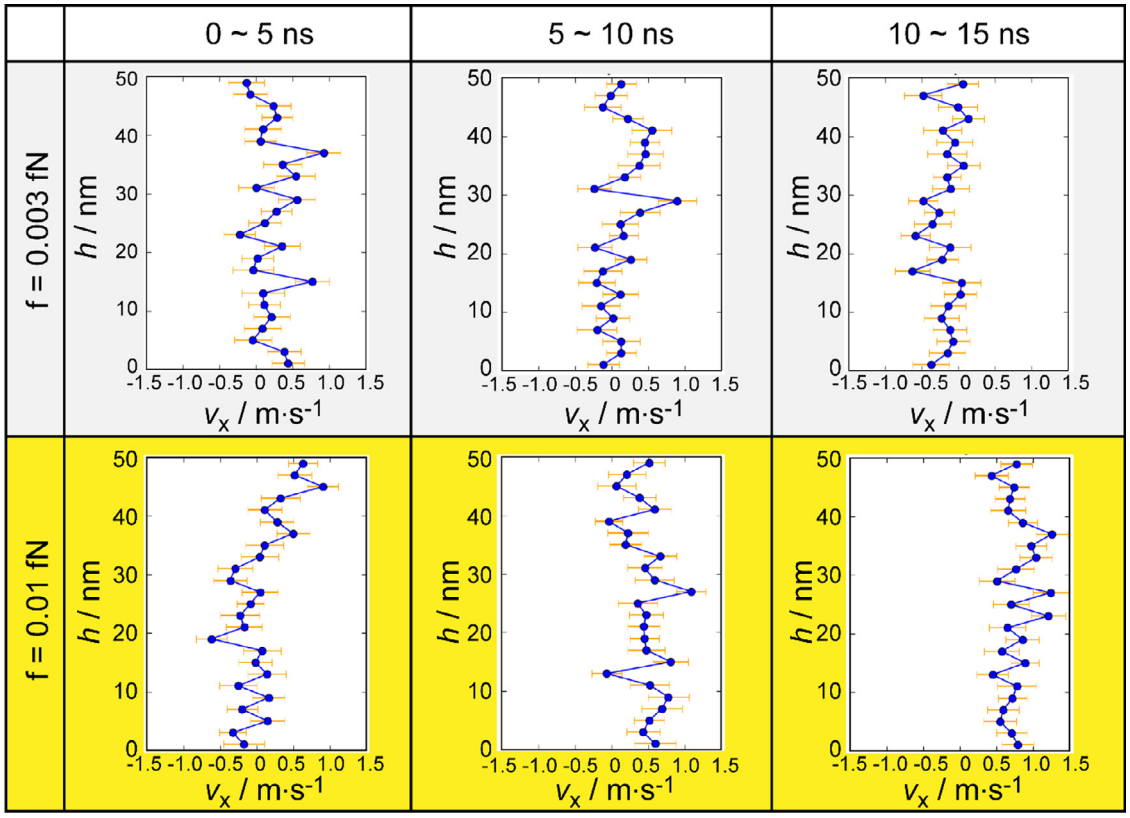

Fig. 4. Fluctuating velocity distributions along the height at consecutive instants for both physiological and accelerating flow cases.

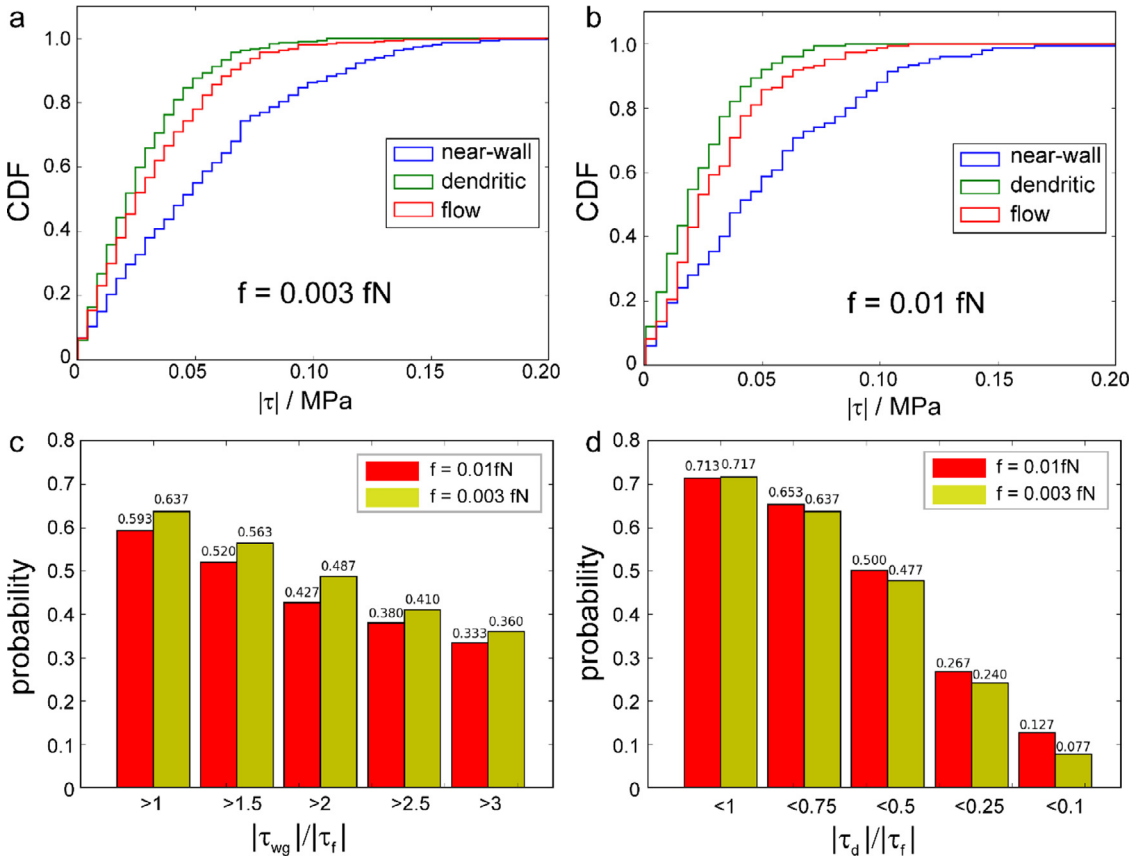

Fig. 5. Distributions of shear stress magnitudes for physiological and accelerating flow cases, and dissections of near-wall and dendritic shear stresses. (a) Cumulative density function (CDF) for shear stress magnitude in the physiological flow case (f = 0.003 fN). (b) CDF for shear stress magnitude in the accelerating flow case (f = 0.01 fN). (c) Dissection of enhanced shear stress in the near-wall region for both cases. (d) Dissection of impaired shear stress in the dendritic region for both cases.

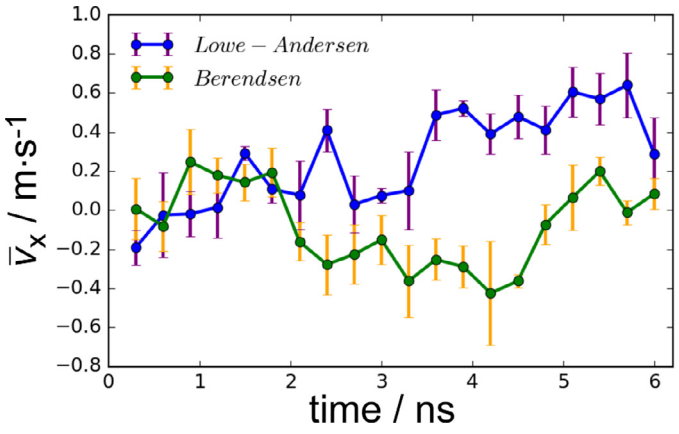

Fig. 6. Average bulk flow velocity evolutions under Lowe-Andersen and Berendsen thermostats.

the desired temperature. To be specific, when velocity is higher than the value to maintain the targeted temperature, an "artificial" force can be regarded to be imposed on the atoms to decelerate the motions of atoms, thereby maintaining the constant temperature. The rescaling of particle velocities may account for the deterioration of average bulk flow velocities under the Berendsen thermostat in Fig. 6. In contrast, Lowe-Andersen dynamics is a variation of Andersen dynamics whereby the radial relative velocities of atom pairs are randomly modified based on a thermal distribution [21], thus, Lowe-Andersen thermostat is independent of absolute atom velocities.

4.2. Flow and conformations of the glycocalyx

Results in Section 3.2 indicate that a slightly elevated external force on water oxygen atom only contributes to a minor increase in bulk flow velocity without modifying the fluctuating spatial distribution of the velocity. A scrutiny of the conformations of the glycocalyx biomolecules in both the physiological and accelerating flow cases (Fig. 7a and b) reveals no dramatic changes in glycocalyx conformations as flow passes by. The homogeneous layouts of sugar chains sterically disturb the motion of the flow, thereby oscillating the velocity profiles along the height. However, if the external force increases to 0.001 pN, as in Ref. [8], the layouts of sugar chains turn to heterogeneous and significant deformation of the glycocalyx biomolecules can be observed (Fig. 7c). The corresponding velocity in the upper ectodomain region ($h > 25$ nm) can reach 10 m/s (External forces are only imposed on water oxygen atoms in the upper ectodomain region in Ref. [8]), and the bulk velocity dominates over the fluctuating velocity along the height (Fig. 7d).

Cardiovascular diseases are normally associated with the shedding of sugar chains [30], and the initial configuration change caused by the shedding of sugar chains may also affect the flow profiles. Thus, further research regarding the flow under different initial glycocalyx configurations is of great importance. On-going studies are undertaken to investigate the flow profiles under situations with varying sugar chain numbers.

5. Conclusions

In this research, large-scale molecular dynamics simulations were conducted to study the flow over the complex structure of the endothelial glycocalyx. A work flowchart regarding procedure of conducting flow/glycocalyx simulation using the MD method was first proposed. Following the procedure, both the physiological and accelerating flow cases were established. Comparisons of velocity and shear stress distributions between both cases were undertaken to unveil the influence of the dendritic structure of the glycocalyx on flow profiles. Besides, the selection of thermostat algorithms was discussed.

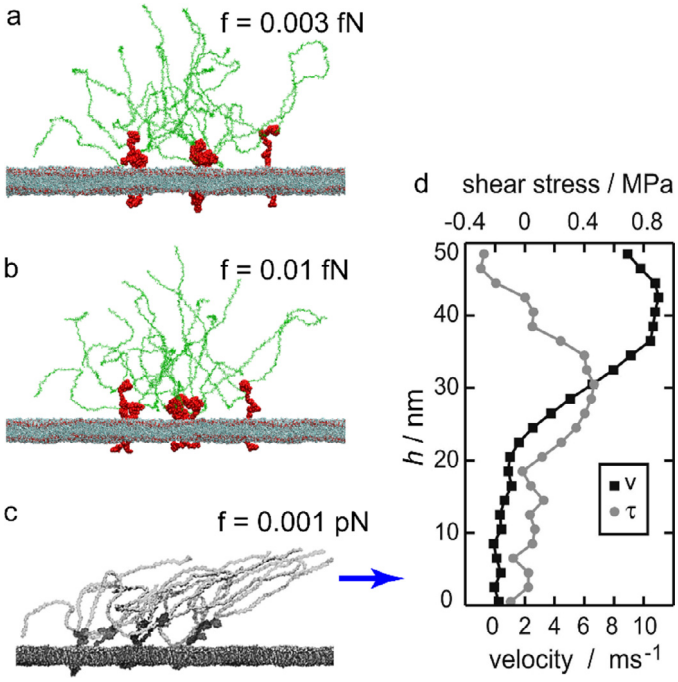

Fig. 7. Typical conformations of the glycocalyx under varying external forces and velocity distribution from a previous study [8]. (a) & (b): Snapshots of typical glycocalyx conformations in the physiological (a) and accelerating (b) flow cases. (c) & (d): Significant conformational changes of the glycocalyx and velocity distribution in an extra-accelerating case from Ref. [8]. Reprinted with permission from Elsevier.

Results have shown that the velocity oscillates around a nearly zero mean along the height in the presence of the dendritic glycocalyx. When the flow forcing is large enough, the bulk flow was accelerated and the flow fluctuation was suppressed. Distributions of shear stress magnitude among the three sub-regions indicate that shear stress is enhanced near the lipid surface but is impaired in the dendritic region where sugar chains gather. Furthermore, comparisons of velocity evolutions under two widely used thermostats imply that the Lowe-Andersen algorithm is a suitable one for flow problems.

This research demonstrates the feasibility to use large-scale molecular dynamics simulations to investigate physiologically relevant complex phenomena, which complements experiments and continuum-based computational methods. The results shed light on the interactions between fluid and biomolecular structures, leading to new insights at the interface between fluid mechanics and physiology.

Acknowledgments

This work was supported by the UK Engineering and Physical Sciences Research Council under the project UK Consortium on Mesoscale Engineering Sciences (UKCOMES) (Grant No. EP/L00030X/1). The first author gratefully acknowledges full support from a Dean's Prize Scholarship from the Faculty of Engineering Sciences, University College London.

References

[1] Pries AR, Secomb TW, Gaehtgens P. The endothelial surface layer. Pflugers Arch 2000;440:653–66.

[2] Alphonsus CS, Rodseth RN. The endothelial glycocalyx: a review of the vascular barrier. Anaesthesia 2014;69:777–84.
[3] Perrin RM, Harper SJ, Bates DO. A role for the endothelial glycocalyx in regulating microvascular permeability in diabetes mellitus. Cell Biochem Biophys 2007;49:65–72.
[4] Schott U, Solomon C, Fries D, Bentzer P. The endothelial glycocalyx and its disruption, protection and regeneration: a narrative review. Scand J Trauma Resusc Emerg Med 2016;24:48.
[5] Reitsma S, Slaaf DW, Vink H, van Zandvoort MA, oude Egbrink MG. The endothelial glycocalyx: composition, functions, and visualization. Pflugers Arch 2007;454:345–59.
[6] Rabelink TJ, de Zeeuw D. The glycocalyx-linking albuminuria with renal and cardiovascular disease. Nat Rev Nephrol 2015;11:667–76.
[7] Ebong EE, Macaluso FP, Spray DC, Tarbell JM. Imaging the endothelial glycocalyx in vitro by rapid freezing/freeze substitution transmission electron microscopy. Arterioscler Thromb Vasc Biol 2011;31:1908–15.
[8] Cruz-Chu ER, Malafeev A, Pajarskas T, Pivkin IV, Koumoutsakos P. Structure and response to flow of the glycocalyx layer. Biophysical Journal 2014;106:232–43.
[9] Jiang XZ, Gong H, Luo KH, Ventikos Y. Large-scale molecular dynamics simulation of coupled dynamics of flow and glycocalyx: towards understanding atomic events on an endothelial cell surface. J R Soc Interface 2017:14.
[10] Yamamoto T, Ogasawara Y, Kimura A, Tanaka H, Hiramatsu O, Tsujioka K, et al. Blood velocity profiles in the human renal artery by Doppler ultrasound and their relationship to atherosclerosis. Arterioscl Throm Vas 1996;16:172–7.
[11] Jorgensen WL, Chandrasekhar J, Madura JD, Impey RW, Klein ML. Comparison of simple potential functions for simulating liquid water. J Chem Phys 1983;79:926–35.
[12] MacKerell AD, Bashford D, Bellott M, Dunbrack RL, Evanseck JD, Field MJ, et al. All-atom empirical potential for molecular modeling and dynamics studies of proteins. J Phys Chem B 1998;102:3586–616.
[13] Allen MPA, Tildesley DJ. Computer simulation of liquids. New York: Oxford University Press; 1987.
[14] Darden T, York D, Pedersen L. Particle mesh Ewald: an N·log(N) method for Ewald sums in large systems. J Chem Phys 1993;98:10089–92.
[15] Miyamoto S, Kollman PA. Settle – an analytical version of the shake and rattle algorithm for rigid water models. J Comput Chem 1992;13:952–62.
[16] Phillips JC, Braun R, Wang W, Gumbart J, Tajkhorshid E, Villa E, et al. Scalable molecular dynamics with NAMD. J Comput Chem 2005;26:1781–802.
[17] Humphrey W, Dalke A, Schulten K. VMD: Visual molecular dynamics. J Mol Graph Model 1996;14:33–8.
[18] Angel Gonzalez M, Abascal JLF. The shear viscosity of rigid water models. J Chem Phys 2010:132.
[19] Gabe IT, Gault JH, Ross J, Mason DT, Mills CJ, Schillingford JP, et al. Measurement of instantaneous blood flow velocity and pressure in conscious man with a catheter-tip velocity probe. Circulation 1969;40:603–14.
[20] Tarbell JM, Shi ZD. Effect of the glycocalyx layer on transmission of interstitial flow shear stress to embedded cells. Biomech Model Mechanobiol 2013;12:111–21.
[21] Lowe CP. An alternative approach to dissipative particle dynamics. Europhys Lett 1999;47:145–51.
[22] Koopman EA, Lowe CP. Advantages of a Lowe-Andersen thermostat in molecular dynamics simulations. J Chem Phys 2006;124:204103.
[23] Berendsen HJC, Postma JPM, Vangunsteren WF, Dinola A, Haak JR. Molecular–dynamics with coupling to an external bath. J Chem Phys 1984;81:3684–90.
[24] Kotsalis EM, Walther JH, Koumoutsakos P. Multiphase water flow inside carbon nanotubes. Int J Multiphas Flow 2004;30:995–1010.
[25] Nicholls WD, Borg MK, Lockerby DA, Reese JM. Water transport through (7,7) carbon nanotubes of different lengths using molecular dynamics. Microfluid Nanofluid 2012;12:257–64.
[26] Hummer G, Rasaiah JC, Noworyta JP. Water conduction through the hydrophobic channel of a carbon nanotube. Nature 2001;414:188–90.
[27] Thomas M, Corry B. Thermostat choice significantly influences water flow rates in molecular dynamics studies of carbon nanotubes. Microfluid Nanofluid 2015;18:41–7.
[28] Basconi JE, Shirts MR. Effects of temperature control algorithms on transport properties and kinetics in molecular dynamics simulations. J Chem Theory Comput 2013;9:2887–99.
[29] Krishnan TVS, Babu JS, Sathian SP. A molecular dynamics study on the effect of thermostat selection on the physical behavior of water molecules inside single walled carbon nanotubes. J Mol Liq 2013;188:42–8.
[30] Tarbell JM, Simon SI, Curry FR. Mechanosensing at the vascular interface. Annu Rev Biomed Eng 2014;16:505–32.